JGR Space Physics

RESEARCH ARTICLE
10.1029/2021JA029524

Multi-Point Observation of Hiss Emerging From Lightning Whistlers

Ondřej Santolík[1,2], Ivana Kolmašová[1,2], Jolene S. Pickett[3], and Donald A. Gurnett[3]

[1]Department of Space Physics, Institute of Atmospheric Physics of the Czech Academy of Sciences, Prague, Czechia, [2]Faculty of Mathematics and Physics, Charles University, Prague, Czechia, [3]Department of Physics and Astronomy, University of Iowa, Iowa City, IA, USA

Key Points:

- We use multi-point measurements of electromagnetic field fluctuations by the cluster space fleet to discuss sources of plasmaspheric hiss
- Our case study shows hiss which was triggered in the dayside outer plasmasphere by unducted whistlers emitted from strong lightning strokes
- Spectral properties of magnetospherically reflecting whistlers and hiss strongly depend on geographical location of the source thunderstorm

Correspondence to:
O. Santolík,
os@ufa.cas.cz

Citation:
Santolík, O., Kolmašová, I., Pickett, J. S., & Gurnett, D. A. (2021). Multi-point observation of hiss emerging from lightning whistlers. *Journal of Geophysical Research: Space Physics*, *126*, e2021JA029524. https://doi.org/10.1029/2021JA029524

Received 30 APR 2021
Accepted 3 NOV 2021

Author Contributions:
Conceptualization: Ondřej Santolík, Ivana Kolmašová
Data curation: Jolene S. Pickett
Formal analysis: Ondřej Santolík, Ivana Kolmašová
Funding acquisition: Ondřej Santolík, Ivana Kolmašová, Jolene S. Pickett, Donald A. Gurnett
Investigation: Ondřej Santolík, Ivana Kolmašová
Methodology: Ondřej Santolík, Ivana Kolmašová
Project Administration: Ondřej Santolík, Jolene S. Pickett
Software: Ondřej Santolík, Ivana Kolmašová

Abstract We analyze continuous multi-point measurements of electromagnetic field waveforms onboard the Cluster spacecraft in order to contribute to the discussion on sources of plasmaspheric hiss, known as a shaping agent for the Earth radiation belts. In our case study we aim at finding sources of hiss observed close to the geomagnetic equator in the outer plasmasphere on the dayside. We find hiss to be triggered from whistlers of different spectral properties. Whistlers with the lowest observed dispersion arrive to different spacecraft with time delays indicating their origin in the northern hemisphere. Positions of source lightning discharges are then found using the time coincidences with the Word Wide Lightning Location Network data from three active thunderstorm regions in Europe. We find that subionospheric propagation of lightning atmospherics is necessary to explain the observations. Geographic locations of their ionospheric exit points then determine spectral properties of resulting unducted whistlers and triggered hiss. By this well documented chain of events starting with a lightning discharge in the atmosphere we confirm that magnetospherically reflecting whistlers and hiss triggered from them are among possible sources of plasmaspheric hiss.

1. Introduction

Plasmaspheric hiss occurs in high plasma density regions surrounding the Earth as band-limited whistler mode waves (Dunckel and Helliwell, 1969; Russell et al., 1969; Thorne et al., 1973) with a well-defined intensity maximum at frequencies near a few hundred herz and on the dayside (Li et al., 2015; Meredith et al., 2018; Spasojevic et al., 2015).

These waves strongly influence the dynamics of the radiation belts (Van Allen, 1959), causing pitch angle diffusion and subsequent losses of electrons to the atmosphere (Kennel and Petschek, 1966), especially from the slot region between the inner and outer radiation belts (Lyons et al., 1972). These effects are highly variable (Watt et al., 2019; Zhu et al., 2021) and organized by the position of the plasmapause (Malaspina et al., 2020). Hiss acts together with other wave emissions also in the outer radiation belt (Drozdov et al., 2020), occurring at larger radial distances in plasmaspheric drainage plumes (Zhang et al., 2019).

The origin of plasmaspheric hiss is still under debate. Thorne et al. (1973, 1979) originally proposed a mechanism of the in situ growth and amplification starting from background electromagnetic turbulence. Church and Thorne (1983) found this mechanism unlikely and suggested the need for an embryonic source which would initiate the electron cyclotron resonant growth. The in situ amplification is, at least in some cases, supported by in situ observations of the amplification rate (Solomon et al., 1988) or by observations of hiss propagating to both hemispheres from the equatorial region close to the plasmapause (Parrot and Lefeuvre, 1986; Santolík et al., 2001) or in plasmaspheric plumes (Laakso et al., 2015). Other cases when hiss propagated close to the whistler mode resonance cone in the equatorial region are not easily reconcilable with this hypothesis (Storey et al., 1991).

Church and Thorne (1983) proposed three possibilities for the embryonic source of plasmaspheric hiss:

1. Chorus emissions (Storey, 1953) entering the plasmasphere at high latitude (see also Bortnik et al., 2011; Hartley et al., 2019, and references therein).
2. The low-frequency component of ducted whistlers that originate in lightning activity (Storey, 1953).
3. Auroral hiss (Gurnett and O'Brien, 1964) entering near the ionospheric foot of the plasmasphere and propagating into the plasmasphere via the magnetospherically reflected whistler mode.

Supervision: Ondřej Santolík, Donald A. Gurnett
Validation: Ondřej Santolík, Ivana Kolmašová, Jolene S. Pickett, Donald A. Gurnett
Writing – original draft: Ondřej Santolík

Concerning the second suggestion of Church and Thorne (1983) for the embryonic source of plasmaspheric hiss, Sonwalkar and Inan (1989) reported that also magnetospherically reflected whistlers (Edgar, 1976; Kimura, 1966; Smith and Angerami, 1968) often trigger hiss emissions and therefore serve as an embryonic source. Draganov et al. (1993) put forward a hypothesis that simple accumulation of many nonducted whistlers can explain the presence of hiss in the plasmasphere. Green et al. (2005) showed that longitudinal, seasonal, and local time distribution of the hiss intensity is similar to the distribution of lightning, with a conclusion that lightning is the dominant source for plasmaspheric hiss. In the follow-up discussion, Meredith et al. (2006) concluded that there is no relation between whistlers and hiss under 2 kHz on the global scale. However, results of Green et al. (2005) have been recently supported by Záhlava et al. (2019), and both the ray tracing simulation of Bortnik et al. (2003a, 2003b) and recent experimental results of Green et al. (2020) showed a significant contribution of whistlers at frequencies below 2 kHz.

Santolík and Chum (2009) suggested that at different times plasmaspheric hiss may arise by different mechanisms, while none of them can explain all the obtained observations. To contribute to this discussion, we have reexamined the mechanism of Sonwalkar and Inan (1989), using the multi-point data recorded by the WBD instruments on Cluster 1, 3, and 4 spacecraft during the close separation campaign on 4th July 2013, when all three Cluster spacecraft recorded the same sequence of lightning generated whistlers which induced hiss bands. We combine the spacecraft measurements with data from the ground based World Wide Lightning Location Network. We confirm that whistlers generated from mid-latitude storms are among possible sources of plasmaspheric hiss below 2 kHz but our case study is unable to address the problem of a long term relative importance of different possible sources of hiss. Section 2 is devoted to the description of our data set, Section 3 shows results of a detailed analysis of the observed whistlers, and Section 4 describes their source lightning discharges. The results are discussed in Section 5, and Section 6 contains brief conclusions of our study.

2. Data

The present study is based on the Wide Band Data (WBD) instruments onboard the Cluster spacefleet (Gurnett et al., 1997, 2001), which primarily provide us with multi-point measurements of fluctuations of the electric field detected by one of the 88 m long double probe electric field antennas (Gustafsson et al., 1997) with effective lengths of 52–53 m (Béghin et al., 2005). The input of the WBD instruments can be alternatively switched to the signals from one of the search coil sensors (Cornilleau-Wehrlin et al., 1997).

Direct telemetry transmissions of real time data from the WBD instruments were received by the NASA Deep Space Network (DSN) stations before October 2007, when two 10-m dishes of the Panska Ves telemetry station (operated by the Institute of Atmospheric Physics of the Czech Academy of Sciences) have been added to the telemetry receiving network. Starting January 2015, only Panska Ves station receives the real time WBD telemetry. Another downlink possibility is to record data at a decreased rate into the onboard memory during the burst mode operations, and channel them eventually to the ESA ground stations together with the telemetry of other Cluster instruments.

During the analyzed interval on July 4, 2013 between 12:00 and 12:10 UT, Cluster 3 and 4 were approximately 40 km apart and the separation of this pair from Cluster 1 was approximately 500 km. The WBD instruments on Cluster 3 and 4 were switched to a mode, in which the measurements are continuously recorded with a sampling frequency of 27.4 kHz and 8 bits per sample, in a pass band between 25 Hz and 9.5 kHz. Electric field antennas Ey and Ez, which are located in the spin plane, were, respectively, used on Cluster 3 and 4 as sensors, replaced on each spacecraft by the magnetic search coil antenna Bx during the transmission intervals of the active sounder (Décréau et al., 1997). In these cases, the search coil characteristics limit the bandwidth below 4 kHz.

As Cluster 3 and Cluster 4 were at close separations, the real time telemetry streams from both spacecraft were received by a single dish Y (PAN80) of the Panska Ves station. The telemetry of Cluster 1 was acquired through the burst mode operations with the onboard storage, resulting in a data rate reduced to one third of the original value. The records are thus not continuous but form a cycle of ∼40 ms long data intervals followed always by ∼80 ms long gaps. The data structure is otherwise the same as on Cluster 4, with alternating Ez and Bx components.

An overview of the data set is shown in Figure 1. Cluster 3, 4, and 1 move one after the other along roughly the same orbit, crossing successively the magnetic equator from the northern to the southern hemisphere. The

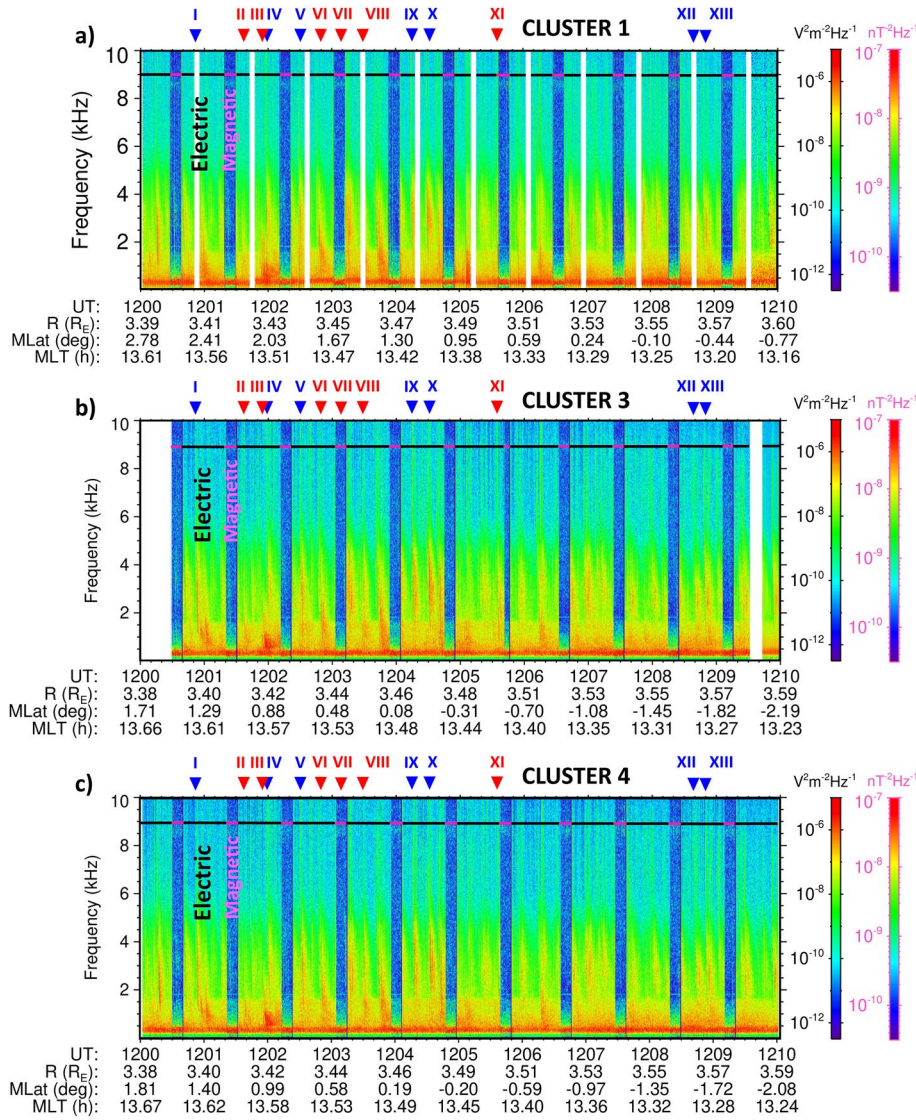

Figure 1. Frequency-time spectrograms obtained from waveform measurements of (a) Cluster 1, (b) Cluster 3, and (c) Cluster 4 on July 4, 2013 between 12:00 and 12:10 UT. Electric and magnetic field measurements are interleaved, as shown by the color coded black-magenta horizontal line on the top of each spectrogram. Representative alternating blocks of electric and magnetic data are indicated near the start of the spectrogram with bold black and magenta colored text, respectively. Magnetic field power spectral densities are given in $nT^2\ Hz^{-1}$, with the corresponding color scales on the right hand side of each spectrogram, while electric field power spectral densities in $V^2\ m^{-2}\ Hz^{-1}$ are coded according to the second color scale from the right. 13 selected intervals of 10 s (according to Table 1) are marked by roman numerals I–XIII on the top of each panel. Blue and red numerals respectively denote the type 1 and type 2 whistlers, examples of which are given in Figure 2. Positions of each spacecraft are given on the bottom of the corresponding panels: radial distance *R* in the Earth radii, magnetic latitude MLat in degrees, and magnetic local time MLT in hours.

measurements were recorded on the dayside, at a radial distance of 3.5 Earth radii. All three spacecraft are still in the plasmasphere with high plasma densities above 80 cm^{-3}, exceeding the upper limit of the active sounder and consistent with a very small potential difference of the probes at the tips of electric antennas relative to the spacecraft body (not shown). The WBD observations are very similar on the three closely separated spacecraft. The measurement cycle with a duration of 52 s repeats approximately synchronously on the three spacecraft, alternating ~10s long magnetic field measurements with the electric field measurements in the remaining part of the cycle. On the time scale of 10 min, shown in Figure 1, we can identify several distinct features. (a) A steady hiss band at few hundreds of Hz is detected by electric and magnetic antennas. (b) Electric antennas detect a weaker and also relatively stable hiss band with an upper frequency cutoff around 1.5 kHz, with a weak counterpart in

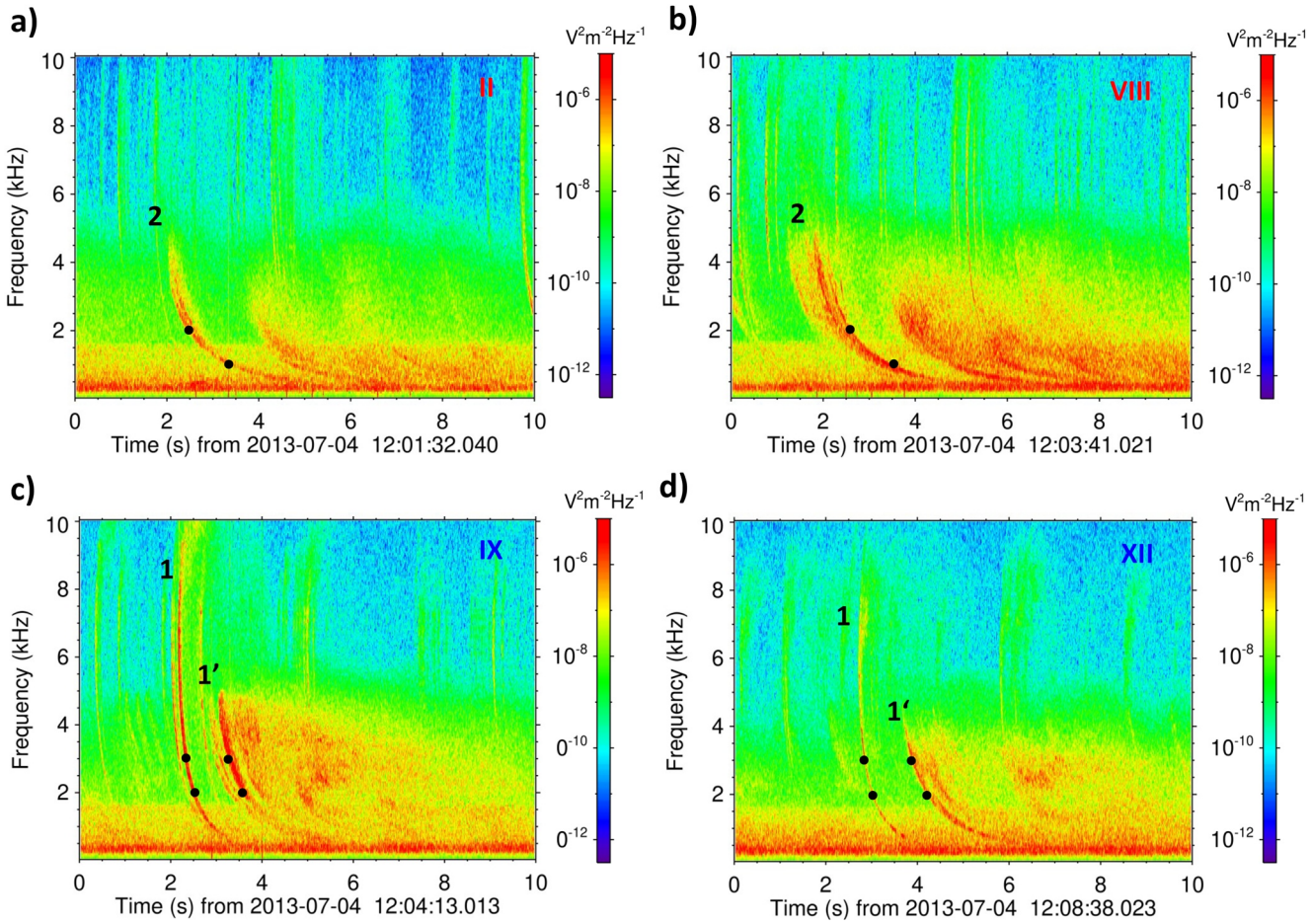

Figure 2. Examples of four selected 10 s intervals, which are respectively marked by II, VIII, IX and XII in the overview Figure 1 (a) and (b) Type 2 whistlers from intervals II and VIII (c) and (d) type 1 whistlers from intervals IX and XII. In all cases, electric field power spectral density is obtained from spectral analysis of waveform data recorded by Cluster 3 by using a 512 point FFT with 50% overlapping and averages over 5 neighboring spectra. Black dots show time delays and frequencies that we use to calculate whistler dispersions for three types of traces: 1, 1', and 2.

the magnetic field measurements. (c) Frequent bursts of broadband hiss detected at the same time by the different spacecraft at frequencies up to 4–5 kHz are also found mainly in the electric field measurements.

3. Whistlers

A closer look at the data on the time scales of several seconds reveals that hiss is accompanied by whistlers which originate from return strokes of lightning discharges in the Earth's atmosphere (Storey, 1953). Whistlers occur throughout the entire analyzed interval. Many of them are overlapping and from those which occur separately we have selected 13 intervals of 10 s which are marked by roman numerals I–XIII in Figure 1.

We have found two distinct patterns in the recorded whistlers which we denote as type 1 and type 2 whistlers. Examples are given in Figure 2, where we show power spectral densities obtained from electric field waveforms recorded by Cluster 3 during intervals II, VIII, IX, and XII. Other spacecraft provide us with very similar spectrograms from these intervals. We can see that the latter two intervals in Figures 2c and 2d contain a distinct whistler trace 1 with a lower dispersion and with a nose frequency (Helliwell, 1965; Helliwell et al., 1956) around 6 kHz, which is, as expected, slightly higher than one quarter of the local electron cyclotron frequency (f_{ce} = 18.8 kHz) obtained from magnetic field measurements onboard the Cluster 3 spacecraft.

Trace 1 is followed by a blurred higher dispersion trace 1', which is accompanied by weaker hiss at frequencies above 2 kHz, sometimes showing also signs of subsequent whistler traces, especially for strong whistlers. These

patterns often repeat in our data set as "type 1" whistlers, occurring 7 times in our selected set of 13 intervals. Intervals in Figures 2a and 2b show blurred whistler traces triggering intense bursts of hiss below 2–3 kHz and followed, for strong whistlers, by one or more traces with higher dispersion. These "type 2" intervals repeat 6 times in the selected set occasionally preceded with a very weak trace with a low dispersion, similar to type 1 trace.

To roughly quantify the observed shapes of whistlers we estimated the dispersion coefficients D for all these whistler traces using the classical method based on the cold plasma approach (Stix, 1992) in a quasi-parallel approximation for a dense plasma, and for propagation along a single path at frequencies well below the nose frequency

$$t = t_0 + t_V + \frac{D}{\sqrt{f}} \quad (1)$$

where t is the time of arrival of the whistler trace at a selected frequency f from an originally broadband source emitting at time t_0, while t_V is the vacuum propagation delay.

We chose frequencies f_1 and f_2 so that the whistler trace can be accurately scanned from the frequency-time spectrograms, and we determined the corresponding times t_1 and t_2. A typical uncertainty of the estimated frequency is around 5 Hz and a typical uncertainty of time estimation ranges from 50 ms (for trace 1) to 100 ms (for traces 1' or 2). This analysis allows us to estimate the dispersion coefficients D and source times t_0 for all the analyzed whistler traces 1, 1', and 2. The results, based on Cluster 3 data from the 13 selected intervals, are summarized in Table 1.

The average dispersion coefficient from all trace 1 results is $D_1 = 45 \pm 7$ s$\sqrt{\text{Hz}}$, while the average dispersion coefficient from the trace 1' analysis was $D_{1'} = 90 \pm 5$ s$\sqrt{\text{Hz}}$. Analysis of type 2 whistler traces yields a very similar average dispersion coefficient, $D_2 = 93 \pm 3$ s$\sqrt{\text{Hz}}$. This strongly suggests a similar mechanism for the 1' and 2 traces. The simplest possible explanation therefore is that the whistler trace 1 corresponds to a half-hop whistler propagating to the equator from the source lightning directly to the spacecraft, without any reflections. Whistler traces 1' and 2 would then correspond to whistlers after the first magnetospheric reflection, where for type 2 events the rays of the original half-hop whistlers miss the spacecraft position.

To verify this hypothesis on propagation of whistlers and to estimate possible effects of associated hiss it is important to know if the waves are electromagnetic or if some of the observed features correspond to quasi-electrostatic waves. Figure 3 shows data for the intervals where signals of the magnetic search coil antennas were used as the WBD input on the three spacecraft. Frequency-time spectrograms from interval VII in Figures 3a–3c clearly show the magnetic field components of type 2 whistler traces (with a corresponding dispersion coefficient of 91 s$\sqrt{\text{Hz}}$, see Table 1) converging into an intense hiss band at hundreds of hertz, and accompanied by faint signatures of the hiss band with the upper cutoff around 1.5 kHz. Hiss bursts following the whistler traces at frequencies above 2 kHz are also observed.

Spectrograms from interval XI shown in Figures 3d–3f provide us with the opportunity to compare the electric and magnetic components of the measured waves, as the WBD input on Cluster 3 was switched to the magnetic antenna later than on the two other spacecraft. Comparison of power spectral densities of the electric field and magnetic field for hiss at a frequency $f \sim$300 Hz results in a ratio of magnetic to electric field amplitudes $cB/E \sim 50$, where c is the speed of light. This is roughly consistent with the expected value, obtained as

$$cB/E = \frac{f_{pe}}{\sqrt{f\left(f_{ce} - f\right)}} \quad (2)$$

assuming again quasiparallel propagating whistler mode waves in a cold plasma (Stix, 1992) with a density of $\sim$200 cm^{-3} and the corresponding plasma frequency f_{pe}, yielding $cB/E \sim 54$ with the measured electron cyclotron frequency $f_{ce} = 18.8$ kHz. Onboard analysis of measurements by the triaxial search coil sensors (Cornilleau-Wehrlin et al., 1997), averaged over 4 s measurement intervals, indeed indicates a right handed polarization of hiss at 300 Hz. This confirms the presence of whistler mode waves and excludes the presence of the X-mode equatorial noise below the lower hybrid frequency ($f_{lh} \sim 470$ Hz). However, the measured magnetic field fluctuations are not well confined to a single plane so any further propagation analysis in not possible using this data set (not shown).

Table 1
Results of Analysis of 13 Selected Whistler Intervals, See Text for Details

Interval no.	Whistler trace type	Start time UT (hour: min)	Start time UT (s)	t_1 from start time (s)	f_1 (kHz)	t_2 from start time (s)	f_2 (kHz)	D ($s\sqrt{Hz}$)	Estimated UT of the causative lightning (hour: min)	Estimated UT of the causative lightning (s)	WWLLN World Wide Lightning Location Network Corresponding strokes Universal Time	Lat (°N)	Lon (°E)	Peak current (kA)
I	1	12:00	48.019	2.231	3.5	2.365	2.5	43.27	12:00	49.45	12:00:49.326314	59.22	38.29	147
	1'	12:00	48.019	3.867	2	4.200	1.5	96.26						
II	2	12:01	32.040	2.437	2	3.268	1	89.72	12:01	32. 33	12:01:32.150764	47.55	28.33	96
III	2	12:01	50.019	2.762	2	3.663	1	97.28	12:01	50.47	12:01:50.441402	45.63	32.36	163
IV	1	12:01	50.019	7.794	4	8.046	2	38.48	12:01	57.14	12:01:56.891150	57.57	38.59	180
	1'	12:01	50.019	8.983	3	9.355	2	90.66						
V	1	12:02	29.037	0.259	4	0.399	3	57.24	12:02	28.32	12:02:28.607433	59.45	38.86	135
	1'	12:02	29.037	1.468	3	1.860	2	95.53						
VI	2	12:02	46.020	1.719	2	2.560	1	90.80	12:02	45.57	12:02:45.418684	45.13	32.57	213
VII	2	12:03	03.000	2.073	2	2.919	1	91.32	12:03	02.89	none			
VIII	2	12:03	41.021	3.630	2	4.525	1	96.63	12:03	41.35	12:03:41.125780	48.25	26.16	293
IX	1	12:04	13.013	2.310	3	2.511	2	48.99	12:04	14.36	none			
	1'	12:04	13.013	3.324	3	3.680	2	86.76						
X	1	12:04	27.008	3.009	3	3.184	2	42.65	12:04	29.17	12:04:28.979911	59.23	38.34	236
	1'	12:04	27.008	4.089	3	4.466	2	91.88						
XI	2	12:05	34.000	1.136	2	1.987	1	91.85	12:05	33.94	12:05:34.062749	44.54	33.67	60
XII	1	12:08	38.023	2.861	3	3.036	2	42.65	12:08	40. 04	none			
	1'	12:08	38.023	3.890	3	4.227	2	82.13						
XIII	1	12:08	49.025	1.210	3.5	1.267	3	42.09	12:08	49.45	12:08:49.138110	57.45	38.52	247
	1'	12:08	49.025	2.253	3	2.610	2	87.00						

Note. The vacuum propagation delay in Equation 1, $t_V = l_R/c$ was estimated based on typical ray lengths l_R from simulation results in Section 5 at 1 kHz, where c is the speed of light in vacuum: $t_V = 70$ ms and 140 ms, for traces 1 and 2, respectively.

The observed type 2 whistler trace, with a dispersion coefficient of 92 $s\sqrt{Hz}$ (see Table 1) is partly seen in both the electric and magnetic field data but the ratio of magnetic to electric field amplitudes is substantially lower than for the 300 Hz hiss, with $cB/E \sim 20$–30, indicating propagation at large angles between the wave vector and the background magnetic field line. The same holds true for the following reflection and induced hiss at above 2 kHz. Hiss below 1.5 kHz shows even lower values of $cB/E \sim 15$, which indicates propagation closer to the whistler mode resonance angle.

Unfortunately, this comparison is not available for the type 1 whistlers in our data set. Therefore, a question still remains: why do we observe two separate types of lightning whistlers, some of which are clearly able to contribute to hiss both below and above 2 kHz? We start answering this question by analyzing multi-spacecraft measurements. We can benefit from the close separation of Cluster spacecraft and analyze the time of arrival of the nose of the sharp whistler trace 1. A rough calculation of the group velocity based on the cold plasma approximation (Stix, 1992) for quasi-parallel propagation in a dense plasma

$$v_g = \frac{2c}{f_{pe} f_{ce}} \left(f_{ce} - f\right)^{3/2} f^{1/2} \tag{3}$$

yields an expected minimum time delay of one millisecond between Cluster 3 and Cluster 4 at the nose frequency $f = 6$ kHz, for plasma densities above 100 cm^{-3}. Realistically higher plasma densities and oblique propagation only increase this time delay, and it therefore can be detected using the WBD waveform measurements.

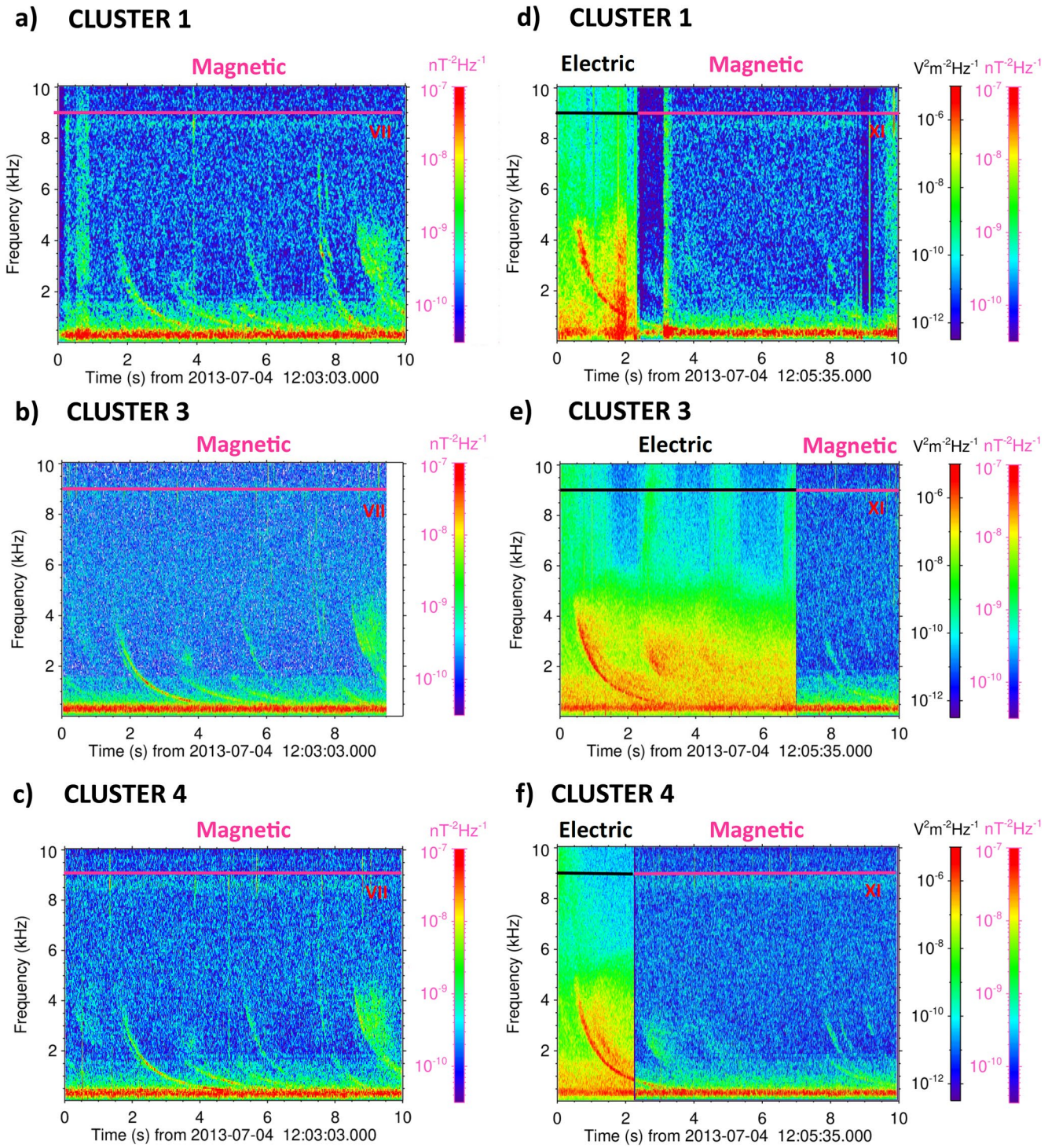

Figure 3. Frequency-time spectrograms obtained from the magnetic field waveforms recorded during interval VII by (a) Cluster 1, (b) Cluster 3, and (c) Cluster 4. Spectrograms from the same three spacecraft for interval XI when the electric field measurements have been switched to the magnetic field at a different time on (e) Cluster 3 than on (d) Cluster 1 and (f) Cluster 4.

Figure 4 shows a type 1 whistler from interval X. Power spectrograms from Cluster 3 and Cluster 4 in Figures 4a and 4b give nearly identical pictures with a sharp first whistler trace, but detailed electric field waveform recordings from both spacecraft in Figure 4c clearly show differences in the initial part of the whistler signature. Both spacecraft detect arrival of strongly modulated sinusoidal signals of the first intensification, with approximately

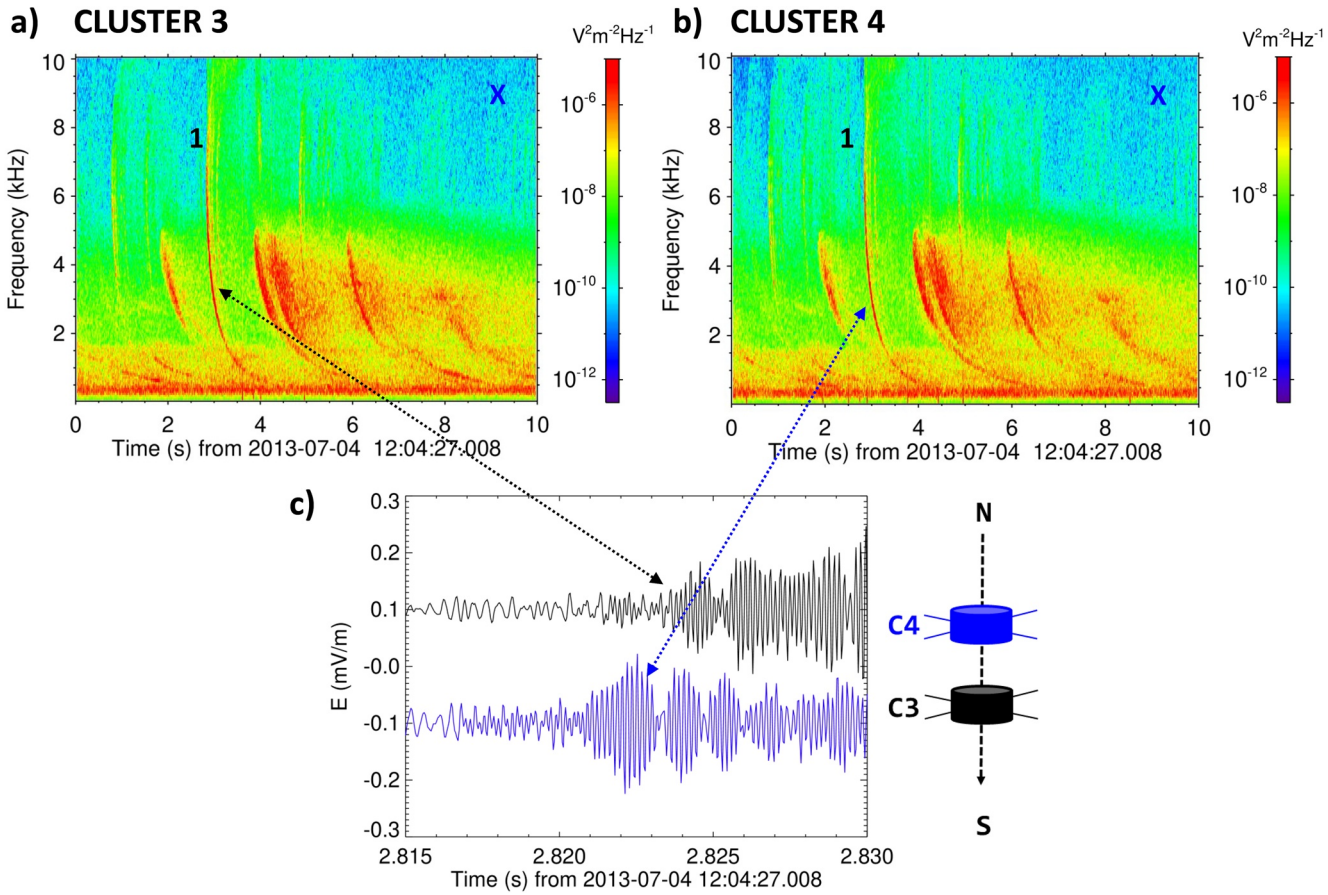

Figure 4. (a) and (b) Electric field power spectral density, which were respectively obtained from spectral analysis of waveform data recorded by Cluster 3 and Cluster 4 during interval X. (c) Initial part of the electric field waveforms of the type 1 whistler trace, shown by a black line for Cluster 3 and by a blue line for Cluster 4.

6 wave periods per millisecond, corresponding well to the estimated nose frequency of 6 kHz. The subsequent amplitude modulation can be explained by beating of coherent monochromatic waves above and below the nose frequency, which arrive later. The time of arrival of the first signal is, as expected, different by a few ms on the two spacecraft, Cluster 4 detecting it first. As Cluster 4 is to the North from Cluster 3, it is clear that the whistlers arrive from the northern hemisphere. This propagation pattern is observed for all first traces in the analyzed intervals of type 1 whistlers.

4. Source Lightning

Assuming that type 1 whistler traces arrive directly from their sources as half-hop whistlers we can identify their source lightning return strokes using the data of one of the ground based lightning location networks. We used the data of the World Wide Lightning Location Network (WWLLNN), which are obtained using time of arrival analysis of signals from very low frequency sensors distributed at 70 different locations around the globe. Their detection efficiency depends on location, time of the day, and strength of the stroke (Hutchins et al., 2012a) but for strong lightning with peak currents larger than 50 kA the absolute efficiency was evaluated to be around 75% over New Zealand (Holzworth et al., 2019).

Over Europe, where the Cluster 3 and Cluster 4 spacecraft have their magnetic footprints during the analyzed parts of their orbits (see the purple line in Figure 5, linked to the real time reception in Panska Ves), the density of the WWLLN detectors is high and we can therefore expect that we would be able to find sources for the majority of whistlers originating in strong discharges. The strength of the discharges was measured by the WWLLN stroke energy, which we converted to the more usual peak current estimator using relations derived by Hutchins et al. (2012b).

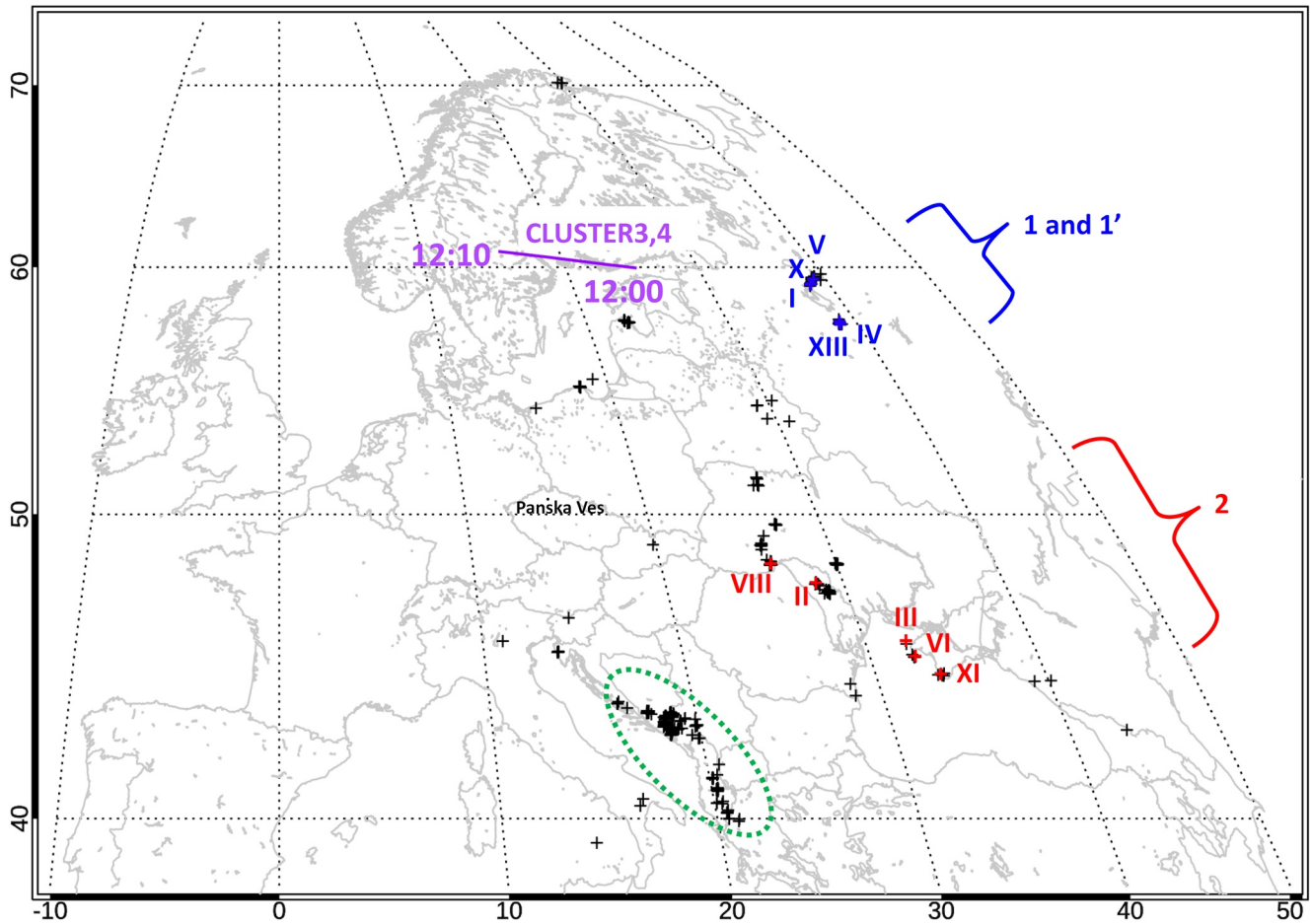

Figure 5. Map of WWLLN lightning locations (shown as black "+" signs) over Europe on July 4, 2013 between 12:00 and 12:10 UT. The magnetic footprints of the Cluster 3 and Cluster 4 orbits (purple line) are nearly identical. Identified source strokes for type 1 and type 2 whistlers are, respectively, shown in blue and red, annotated by the roman numerals corresponding to the analyzed intervals. Strokes from an Adriatic storm at lower latitudes are encircled by a green dotted line.

Black '+' signs in Figure 5 show all WWLLN stroke locations in the geographic region at latitudes above 30°N and longitudes between 10°W and 50°E, obtained on the 4th of July 2013 between 12:00 and 12:10 UT. From this set of 377 individual lightning strokes we have selected those, which have their WWLLN stroke time within 400 ms from the time t_0 obtained from the Cluster 3 data using Equation 1. Out of the analyzed 13 whistler intervals, for 3 we didn't find any corresponding WWLLN stroke, for 2 we found a single corresponding stroke, for 6 we found two candidate strokes, for 1 we found three strokes, and for the remaining one four strokes.

In these cases, where we obtained two or more possible strokes fulfilling our criterion, all but one corresponded to multiple strokes from the same lightning flash at the same location. We have then selected the strongest stroke, which always was the first one in the sequence. Table 1 summarizes the positions and equivalent peak currents of these estimated source strokes. Their positions are plotted in Figure 5 which clearly shows that the causative lightning return strokes for type 1 whistlers are found closer to the magnetic footprint of the spacecraft, at higher geographic latitudes of 57.5°–59.5°N, corresponding to 53.0°–54.8° of the geomagnetic dipole latitude. The causative lightning return strokes of type 2 whistlers are found at lower latitudes of 44.5°–48.3°N (41.1°–45.9° of the geomagnetic dipole latitude). We also found an intense thunderstorm activity in the Adriatic region between 40° and 43.5°N (38.9°–43° of the geomagnetic dipole latitude).

Noting that the sources are displaced from the spacecraft magnetic footprint, we expect that only strong lightning strokes can feed sufficient electromagnetic energy into the Earth-ionosphere waveguide, so that the resulting atmospherics can travel to a distant exit point and generate the observed whistlers. Relation of the equivalent peak current of the identified source strokes for the type 1 and type 2 whistlers to the overall distribution of peak

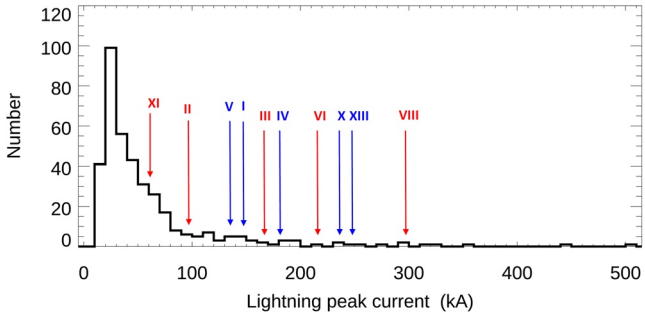

Figure 6. Histogram of WWLLN equivalent peak currents obtained from 377 lightning strokes shown as black "+" signs in Figure 5. Arrows with roman numerals show the peak currents of identified source strokes for the type 1 (blue) and type 2 (red) whistlers.

currents in the analyzed geographical region and time interval is given in Figure 6. The results confirm that the whistler source lightning strokes tend to be placed on the tail of the distribution at high peak currents, with no clear differences of the source peak currents for the two types of whistlers.

5. Discussion

Although source lightning discharges of the type 2 whistlers are located at larger distances from the spacecraft magnetic footprint (1,400–1,900 km) compared to sources of the type 1 whistlers (800 and 1,300 km), they do not tend to be generated by stronger lightning. At the same time, the spectral forms of the two types of whistlers are different. A plausible explanation of both these observations is as follows:

1. The lightning discharges generate atmospherics with a broadband frequency spectrum which propagate in the Earth-ionosphere waveguide to all horizontal directions radially from their source.
2. Part of their electromagnetic power continuously leaks into the ionosphere during this subionospheric propagation.
3. The leaked power quickly decreases with the distance of the ionospheric exit point from the source lightning discharge but the measurable affected area has a radius of at least 2,000 km around a strong lightning (Burkholder et al., 2013; Fišer et al., 2010).
4. The Snell's law implies wave vector directions which are very close to the local vertical direction at the exit points, determining thus boundary conditions for their subsequent propagation into the magnetosphere.
5. The waves propagate in an unducted mode (Edgar, 1976; Kimura, 1966; Santolík et al., 2009; Shklyar and Jiříček, 2000; Smith and Angerami, 1968) upward from their exit points, each frequency along a slightly different path.
6. The type 1 whistler traces observed by the spacecraft correspond to the half-hop propagation from the ionosphere to the equator: the whistlers are then composed of different frequencies from the same source, each of them arriving from a slightly different ionospheric exit point at higher latitudes, which the atmospherics from the type 1 source lightning discharges reach with acceptably low attenuation.
7. Another set of ionospheric exit points corresponds to separate frequencies of type 1´ or type 2 whistlers which are observed after the first magnetospheric reflection: lower frequencies observed in type 2 case would also correspond to lower latitudes of the corresponding ionospheric exit points.
8. Hiss bands are triggered by these whistlers (Sonwalkar & Inan, 1989), but also by whistlers reflecting many times in the magnetosphere (Bortnik et al., 2003a, 2003b) where discharges at yet lower latitudes of the Adriatic storm might contribute to triggering of hiss below 1.5 kHz.

To verify if these scenarios are realistic for both types of whistlers we performed a schematic ray-tracing simulation, based on the procedure of Cerisier (1970) with a diffusive equilibrium model of the plasma density distribution, modified to include an adaptive integration step by Santolík et al. (2006, 2009). The model in our case was set to an exospheric temperature of 700 K and calibrated to a plasma density of 10^4 cm^{-3} at a reference altitude of 700 km. The wave rays are simulated based on cold plasma theory which doesn't reflect any possible changes of wave amplitudes by wave-particle interactions. This model is necessarily only a crude approximation of the real plasma medium in the magnetosphere but it is sufficient to demonstrate the properties of wave propagation, which lead to the observed effects.

Figure 7a shows that only a relatively narrow interval of 3.2° for ionospheric exit points at higher latitudes is needed to account for an unducted half-hop propagation of different frequency components to a spacecraft located at the magnetic equator at a radial distance of 3.5 Earth radii. The waves arrive with wave vectors that are obliquely inclined from the focal magnetic field line by 58°–60°, which is still sufficiently far from the whistler mode resonance cone to account for the electromagnetic nature of these waves. These rays would correspond to the half-hop (trace 1) part of type 1 whistlers whose source discharges have been detected at higher latitudes. Following the rays past the spacecraft we may notice them undergoing a magnetospheric reflection and returning to the equator at different places far from the spacecraft: low frequencies, represented by the ray at 1 kHz return to

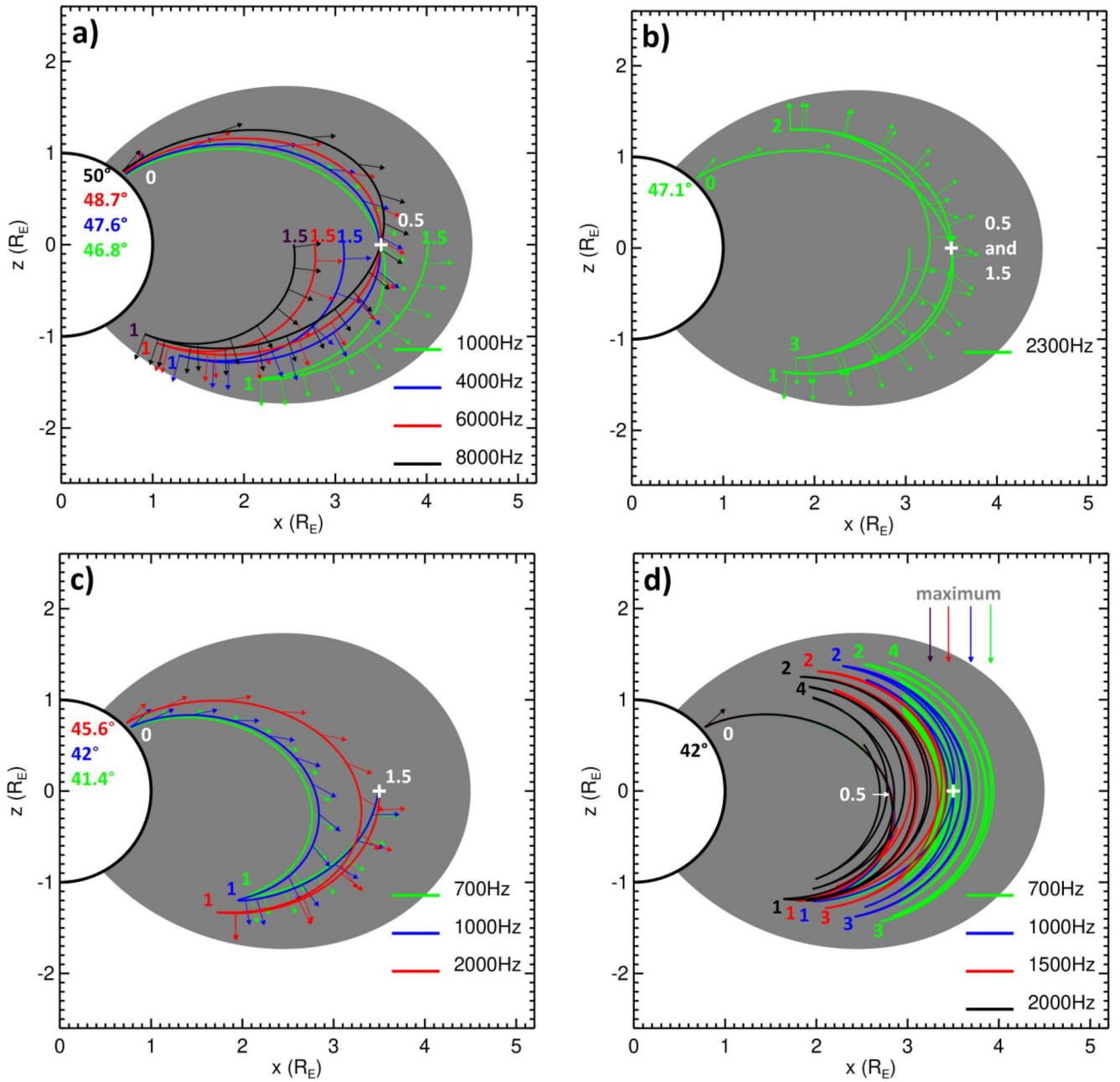

Figure 7. Schematic ray tracing simulation from the ionosphere to the Cluster spacecraft shown by a white "+" sign at the equator and at a radial distance of 3.5 Earth radii. The plot is drawn in the plane of the local magnetic meridian containing the spacecraft position in Cartesian coordinates x-z where z is parallel to the magnetic dipole axis. (a) Type 1 whistler trace for color coded frequencies 1–8 kHz (b) Ray for a frequency of 2.3 kHz (c) Type 2 whistler trace for color coded frequencies 0.7–2 kHz (d) Rays exiting from the geomagnetic dipole latitude of 42° trace for color coded frequencies 0.7–2 kHz during 10s of the group time, with their maximum radial distances shown on the top. Geomagnetic dipole latitudes of the ionospheric exit points of the separate rays are given on the left hand side of each panel. Exit points are marked by white "0", equatorial passes are marked by "0.5" and "1.5," magnetospheric reflections are identified by color coded numbers 1, 2, 3, and 4. Arrows are added to the rays to show the wave vector directions with an interval of 100 ms of the group time. Gray area follows the magnetic field line passing through the equator at a radial distance of 4.5 Earth radii.

larger radial distances, and high frequencies (4, 6, and 8 kHz) return to lower radial distances than the spacecraft position.

A frequency between 1 and 4 kHz must therefore exist, for which the corresponding ray passes through the spacecraft not only as a half-hop whistler but also after the magnetospheric reflection. Figure 7b show such a ray for a

frequency of 2.3 kHz, which would then contribute to both type 1 and type 1' traces. Further evolution of the ray during first three magnetospheric reflections indicates that the waves gradually move to lower radial distances.

Figure 7c corresponds to possible propagation of type 2 whistlers. Waves at frequencies below 2.3 kHz, all of them launched from lower latitudes than in the previous case, initially miss the spacecraft position and converge at the spacecraft location only after the first magnetospheric reflection. Their wave vector directions at that point are inclined by 77°–79° from the local field line. This is still far enough (5°–11°) from the resonance cone, which explains the observed electromagnetic nature of these waves. Occasional very weak half-hop whistlers preceding the type 2 traces could be explained by a long propagation and strong attenuation of the lightning generated atmospherics in the Earth-ionosphere waveguide.

Finally, a long lasting hiss emission below 1.5 kHz might be, at least in part, attributed to sources from whistlers originating in the Adriatic storm at geomagnetic latitudes below 43°. Unducted whistlers can bounce in the magnetosphere back and forth with many reflections. Bortnik et al. (2003a, 2003b) showed that the lifetime of these waves is limited by the wave damping caused by the low energy component of the electron distribution function. At the equatorial distance of 3.5 Earth radii, their results give lifetimes of at least 20 s, which accounts for many reflections. Figure 7d shows rays propagating for 10 s from an exit point at a geomagnetic latitude of 42°, from which the 2 kHz waves always stay at lower radial distances and do not reach the spacecraft but waves below 1.5 kHz propagate to larger radial distances up to the spacecraft position.

6. Conclusions

Detailed analysis of high cadence multi-point measurements of electromagnetic field by the Cluster spacefleet allowed us to reconstruct the chain of events leading to the occurrence of triggered hiss in the outer edge of the equatorial dayside plasmasphere. Sources of triggering waves for these emissions are found in lightning discharges localized by the Word Wide Lightning Location Network to different thunderstorms spread over 15° of geomagnetic latitude. The location of the source lighting determines the spectral shapes and frequencies of the resulting unducted whistlers. Our case study demonstrates that lightning whistlers penetrating the ionosphere at latitudes around 40° of geomagnetic latitude and propagating unducted should be considered as one of the sources of plasmaspheric hiss below 2 kHz.

Data Availability Statement

The data supporting the conclusions of this study can be obtained from the European Space Agency's Cluster Science Archive on https://www.cosmos.esa.int/web/csa. The World Wide Lightning Location Network (WWLLN) data are available for sale from the University of Washington (http://wwlln.net/).

Acknowledgments
We thank our colleagues at the Panská Ves station (Jakub Horký, Jiří Šimůnek, Michal Siman, and Jiří Baše) for their tireless work on receptions of the Cluster WBD direct telemetry. We are especially grateful for the work of the late Jan Šmilauer who was at the beginning of this effort. The work on the present paper has received funding from the European Union's Horizon 2020 research and innovation programme under grant agreement 870437 (SafeSpace), from the GAČR grant 20-09671S, and from the MSMT grant LTAUSA17070.

References

Béghin, C., Décréau, P. M. E., Pickett, J., Sundkvist, D., & Lefebvre, B. (2005). Modeling of cluster's electric antennas in space: Application to plasma diagnostics. *Radio Science*, *40*, RS6008. https://doi.org/10.1029/2005RS003264

Bortnik, J., Chen, L., Li, W., Thorne, R. M., Meredith, N. P., & Horne, R. B. (2011). Modeling the wave power distribution and characteristics of plasmaspheric hiss. *Journal of Geophysical Research*, *116*, A12209. https://doi.org/10.1029/2011JA016862

Bortnik, J., Inan, U. S., & Bell, T. F. (2003a). Frequency-time spectra of magnetospherically reflecting whistlers in the plasmasphere. *Journal of Geophysical Research*, *108*, 1030. https://doi.org/10.1029/2002JA009387

Bortnik, J., Inan, U. S., & Bell, T. F. (2003b). Energy distribution and lifetime of magnetospherically reflecting whistlers in the plasmasphere. *Journal of Geophysical Research*, *108*, 1199. https://doi.org/10.1029/2002JA009316

Burkholder, B. S., Hutchins, M. L., McCarthy, M. P., Pfaff, R. F., & Holzworth, R. H. (2013). Attenuation of lightning-produced sferics in the Earth-ionosphere waveguide and low-latitude ionosphere. *Journal of Geophysical Research: Space Physics*, *118*, 3692–3699. https://doi.org/10.1002/jgra.50351

Cerisier, J. (1970). Propagation perpendiculaire au voisinage de la fréquence de la résonance hybride basse In *Plasma waves in space and in the laboratory* (Vol. 2, pp. 487–521). Edinburgh University Press.

Church, S. R., & Thorne, R. M. (1983). On the origin of plasmaspheric hiss: Ray path integrated amplification. *Journal of Geophysical Research*, *88*(A10), 7941–7957. https://doi.org/10.1029/JA088iA10p07941

Cornilleau-Wehrlin, N., Chauveau, P., Louis, S., Meyer, A., Nappa, J. M., Perraut, S., et al. (1997). The cluster spatio-temporal analysis of field fluctuations (STAFF) experiment. *Space Science Reviews*, *79*, 107–136. https://doi.org/10.1023/A:1004979209565

Décréau, P. M. E., Fergeau, P., Krannosels'kikh, V., Lévêque, M., Martin, Ph., Randriamboarison, O., et al. (1997). *Space Science Reviews*, *79*, (1/2), 157–193. http://dx.doi.org/10.1023/a:1004931326404

Draganov, A. B., Inan, U. S., Sonwalkar, V. S., & Bell, T. F. (1993). Whistlers and plasmaspheric hiss: Wave directions and three-dimensional propagation. *Journal of Geophysical Research*, *98*(A7), 11401–11410. https://doi.org/10.1029/93JA00662

Drozdov, A. Y., Usanova, M. E., Hudson, M. K., Allison, H. J., & Shprits, Y. Y. (2020). The role of hiss, chorus, and EMIC waves in the modeling of the dynamics of the multi-MeV radiation belt electrons. *Journal of Geophysical Research: Space Physics*, *125*, e2020JA028282. https://doi.org/10.1029/2020JA028282

Dunckel, N., & Helliwell, R. A. (1969). Whistler-mode emissions on the OGO 1 satellite. *Journal of Geophysical Research*, *74*(26), 6371–6385. https://doi.org/10.1029/JA074i026p06371

Edgar, B. C. (1976). The upper- and lower-frequency cutoffs of magnetospherically reflected whistlers. *Journal of Geophysical Research*, *81*(1), 205–211. https://doi.org/10.1029/JA081i001p00205

Fišer, J., Chum, J., Diendorfer, G., Parrot, M., & Santolík, O. (2010). Whistler intensities above thunderstorms. *Annales Geophysicae*, *28*, 37–46. https://doi.org/10.5194/angeo-28-37-2010

Green, A., Li, W., Ma, Q., Shen, X.-C., Bortnik, J., & Hospodarsky, G. B. (2020). Properties of lightning generated whistlers based on Van Allen Probes observations and their global effects on radiation belt electron loss. *Geophysical Research Letters*, *47*, e2020GL089584. https://doi.org/10.1029/2020GL089584

Green, J. L., Boardsen, S., Garcia, L., Taylor, W. W. L., Fung, S. F., & Reinisch, B. W. (2005). On the origin of whistler mode radiation in the plasmasphere. *Journal of Geophysical Research*, *110*, A03201. https://doi.org/10.1029/2004JA010495

Gurnett, D. A., Huff, R. L., & Kirchner, D. L. (1997). The wide-band plasma wave investigation. *Space Science Reviews*, *79*, 195–208. https://doi.org/10.1023/A:1004966823678

Gurnett, D. A., Huff, R. L., Pickett, J. S., Persoon, A. M., Mutel, R. L., Christopher, I. W., et al. (2001). First results from the cluster wideband plasma wave investigation. *Annales Geophysicae*, *19*, 1259–1272. https://doi.org/10.5194/angeo-19-1259-2001

Gurnett, D. A., & O'Brien, B. J. (1964). High-latitude geophysical studies with satellite Injun 3: 5. Very-low-frequency electromagnetic radiation. *Journal of Geophysical Research*, *69*(1), 65–89. https://doi.org/10.1029/JZ069i001p00065

Gustafsson, G., Boström, R., Holback, B., Holmgren, G., Lundgren, A., Stasiewicz, K., et al. (1997). The electric field and wave experiment for the Cluster mission. *Space Science Reviews*, *79*, 137–156. https://doi.org/10.1023/A:1004975108657

Hartley, D. P., Kletzing, C. A., Chen, L., Horne, R. B., & Santolík, O. (2019). Van Allen probes observations of chorus wave vector orientations: Implications for the chorus-to-hiss mechanism. *Geophysical Research Letters*, *46*, 2337–2346. https://doi.org/10.1029/2019GL082111

Helliwell, R. (1965). *Whistlers and related ionospheric phenomena*. Stanford University Press.

Helliwell, R. A., Crary, J. H., Pope, J. H., & Smith, R. L. (1956). The "nose" whistler—A new high-latitude phenomenon. *Journal of Geophysical Research*, *61*(1), 139–142. https://doi.org/10.1029/JZ061i001p00139

Holzworth, R. H., McCarthy, M. P., Brundell, J. B., Jacobson, A. R., & Rodger, C. J. (2019). Global distribution of superbolts. *Journal of Geophysical Research: Atmosphere*, *124*, 9996–10005. https://doi.org/10.1029/2019JD030975

Hutchins, M. L., Holzworth, R. H., Brundell, J. B., & Rodger, C. J. (2012a). Relative detection efficiency of the world wide lightning location network. *Radio Science*, *47*, RS6005. https://doi.org/10.1029/2012RS005049

Hutchins, M. L., Holzworth, R. H., Rodger, C. J., & Brundell, J. B. (2012b). Far-field power of lightning strokes as measured by the world wide lightning location network. *Journal of Atmospheric and Oceanic Technology*, *29*, 1102–1110. https://doi.org/10.1175/JTECH-D-11-00174.1

Kennel, C. F., & Petschek, H. E. (1966). Limit on stably trapped particle fluxes. *Journal of Geophysical Research*, *71*(1), 1–28. https://doi.org/10.1029/JZ071i001p00001

Kimura, I. (1966). Effects of Ions on Whistler-Mode Ray Tracing. *Radio Science*, *1*, 269–284. https://doi.org/10.1002/rds196613269

Laakso, H., Santolík, O., Horne, R., Kolmašová, I., Escoubet, P., Masson, A., & Taylor, M. (2015). Identifying the source region of plasmaspheric hiss. *Geophysical Research Letters*, *42*, 3141–3149. https://doi.org/10.1002/2015GL063755

Li, W., Ma, Q., Thorne, R. M., Bortnik, J., Kletzing, C. A., Kurth, W. S., et al. (2015). Statistical properties of plasmaspheric hiss derived from Van Allen Probes data and their effects on radiation belt electron dynamics. *Journal of Geophysical Research: Space Physics*, *120*, 3393–3405. https://doi.org/10.1002/2015JA021048

Lyons, L. R., Thorne, R. M., & Kennel, C. F. (1972). Pitch-angle diffusion of radiation belt electrons within the plasmasphere. *Journal of Geophysical Research*, *77*(19), 3455–3474. https://doi.org/10.1029/JA077i019p03455

Malaspina, D. M., Zhu, H., & Drozdov, A. Y. (2020). A wave model and diffusion coefficients for plasmaspheric hiss parameterized by plasmapause location. *Journal of Geophysical Research: Space Physics*, *125*, e2019JA027415. https://doi.org/10.1029/2019JA027415

Meredith, N. P., Horne, R. B., Clilverd, M. A., Horsfall, D., Thorne, R. M., & Anderson, R. R. (2006). Origins of plasmaspheric hiss. *Journal of Geophysical Research*, *111*, A09217. https://doi.org/10.1029/2006JA011707

Meredith, N. P., Horne, R. B., Kersten, T., Li, W., Bortnik, J., Sicard, A., & Yearby, K. H. (2018). Global model of plasmaspheric hiss from multiple satellite observations. *Journal of Geophysical Research: Space Physics*, *123*, 4526–4541. https://doi.org/10.1029/2018JA025226

Parrot, M., & Lefeuvre, F. (1986). Statistical study of the propagation characteristics of ELF hiss observed on GEOS-1, inside and outside the plasmasphere. *Annales Geophysicae*, *4*, 363.

Russell, C. T., Holzer, R. E., & Smith, E. J. (1969). OGO 3 observations of ELF noise in the magnetosphere: 1. Spatial extent and frequency of occurrence. *Journal of Geophysical Research*, *74*(3), 755–777. https://doi.org/10.1029/JA074i003p00755

Santolík, O., & Chum, J. (2009). The origin of plasmaspheric hiss. *Science*, *324*, 729–730. https://doi.org/10.1126/science.1172878

Santolík, O., Chum, J., Parrot, M., Gurnett, D. A., Pickett, J. S., & Cornilleau-Wehrlin, N. (2006). Propagation of whistler mode chorus to low altitudes: Spacecraft observations of structured ELF hiss. *Journal of Geophysical Research*, *111*, A10208.

Santolík, O., Parrot, M., Inan, U. S., Burešová, D., Gurnett, D. A., & Chum, J. (2009). Propagation of unducted whistlers from their source lightning: A case study. *Journal of Geophysical Research*, *114*, A03212. https://doi.org/10.1029/2008JA013776

Santolík, O., Parrot, M., Storey, L. R. O., Pickett, J. S., & Gurnett, D. A. (2001). Propagation analysis of plasmaspheric hiss using Polar PWI measurements. *Geophysical Research Letters*, *28*(6), 1127–1130. https://doi.org/10.1029/2000gl012239

Shklyar, D. R., & Jiříček, F. (2000). Simulation of nonducted whistler spectrograms observed aboard the MAGION 4 and 5 satellites. *Journal of Atmospheric and Solar-Terrestrial Physics*, *62*(5), 347–370. https://doi.org/10.1016/S1364-6826(99)00097-8

Smith, R. L., & Angerami, J. J. (1968). Magnetospheric properties deduced from OGO 1 observations of ducted and nonducted whistlers. *Journal of Geophysical Research*, *73*(1), 1–20. https://doi.org/10.1029/JA073i001p00001

Solomon, J., Cornilleau-Wehrlin, N., Korth, A., & Kremser, G. (1988). An experimental study of ELF/VLF hiss generation in the Earth's magnetosphere. *Journal of Geophysical Research*, *93*(A3), 1839–1847. https://doi.org/10.1029/JA093iA03p01839

Sonwalkar, V. S., & Inan, U. S. (1989). Lightning as an embryonic source of VLF hiss. *Journal of Geophysical Research*, *94*(A6), 6986–6994. https://doi.org/10.1029/JA094iA06p06986

Spasojevic, M., Shprits, Y. Y., & Orlova, K. (2015). Global empirical models of plasmaspheric hiss using Van Allen Probes. *Journal of Geophysical Research: Space Physics*, *120*(12), 10370–10383. https://doi.org/10.1002/2015JA021803

Stix, T. H. (1992). *Waves in plasmas*. Springer (ISBN:978-0-88318-859-0).

Storey, L. R. O. (1953). An investigation of whistling atmospherics. *Philosophical Transactions of the Royal Society of London - Series A: Mathematical and Physical Sciences*, *246*, 113–141. https://doi.org/10.1098/rsta.1953.0011

Storey, L. R. O., Lefeuvre, F., Parrot, M., Cairó, L., & Anderson, R. R. (1991). Initial survey of the wave distribution functions for plasmaspheric hiss observed by ISEE 1. *Journal of Geophysical Research*, *96*(A11), 19469–19489. https://doi.org/10.1029/91JA01828

Thorne, R., Church, S., & Gorney, D. (1979). On the origin of plasmaspheric hiss: The importance of wave propagation and the plasmapause. *Journal of Geophysical Research*, *84*(A9), 5241–5247. https://doi.org/10.1029/JA084iA09p05241

Thorne, R. M., Smith, E. J., Burton, R. K., & Holzer, R. E. (1973). Plasmaspheric hiss. *Journal of Geophysical Research*, *78*(10), 1581–1596. https://doi.org/10.1029/JA078i010p01581

Van Allen, J. A. (1959). The geomagnetically trapped corpuscular radiation. *Journal of Geophysical Research*, *64*(11), 1683–1689. https://doi.org/10.1029/JZ064i011p01683

Watt, C. E. J., Allison, H. J., Meredith, N. P., Thompson, R. L., Bentley, S. N., Rae, I. J., et al. (2019). Variability of quasilinear diffusion coefficients for plasmaspheric hiss. *Journal of Geophysical Research: Space Physics*, *124*, 8488–8506. https://doi.org/10.1029/2018JA026401

Záhlava, J., Nemec, F., Santolík, O., Kolmašová, I., Hospodarsky, G. B., Parrot, M., et al. (2019). Lightning contribution to overall whistler mode wave intensities in the plasmasphere. *Geophysical Research Letters*, *46*, 8607–8616. https://doi.org/10.1029/2019GL083918

Zhang, W., Ni, B., Huang, H., Summers, D., Fu, S., Xiang, Z., et al. (2019). Statistical properties of hiss in plasmaspheric plumes and associated scattering losses of radiation belt electrons. *Geophysical Research Letters*, *46*, 5670–5680. https://doi.org/10.1029/2018GL081863

Zhu, Q., Cao, X., Gu, X., Ni, B., Xiang, Z., Fu, S., et al. (2021). Empirical loss timescales of slot region electrons due to plasmaspheric hiss based on Van Allen Probes observations. *Journal of Geophysical Research: Space Physics*, *126*, e2020JA029057. https://doi.org/10.1029/2020JA029057